# Error Analysis in Multibeam Hydrographic Survey System

Basil Daniel Devote
Department of Surveying and Geomatics,Faculty of Environmental Sciences,
Rivers State University, Port Harcourt, Nigeria.
basil.devote@ust.edu.ng

DOI: https://dx.doi.org/10.4314/sajg.v13i2.2

## Abstract

*Hydrographic surveying involves the integration of a depth-measuring sonar (Sound navigation and ranging) with a positioning system or Global Navigation Satellite System (GNSS); a motion sensor or Inertia Measuring Unit (IMU); and an azimuth sensor (gyroscope). The various sensors acquire data in terms of their respective reference frame and time. The challenge lies in integrating the various sensor frames and time, and in transforming the vessel frame coordinate system into a terrestrial reference frame. The integration of the various sensor frames and time is necessary to minimize systematic errors in the bathymetric data that result from latency, and calibration uncertainty. The focus of this research is to model the systematic bias associated with the integration of the various sensor reference frames. In so doing, the quality of the acquired data is enhanced, and error budgeting and uncertainty prediction can be effectively carried out during the preparation, acquisition, and processing stages of the bathymetric exercise. As such, the required project specification and hydrographic standards, as defined by the International Hydrographic Organization (IHO), are met.*

*Keywords: Error Analysis, Bathymetric Uncertainty, Multibeam Echo Sounder*

## 1. Introduction

A Multibeam Echo Sounder (MBES) is an acoustic Sonar (Sounding Navigation and Ranging) device used to determine the underwater depth of water bodies. MBES generate acoustic waves which are propagated from the transducer through the water column to the seabed and back to the transceiver (Hughes, 2018; Douglas, 2019). The MBES produces a fan-like array of beams, called swathe, which can offer a complete coverage of the seabed morphology. The swathe (beamforming) capabilities of the multibeam system have made it the choice system for deep-sea and ocean mapping, for the mapping of harbors and wrecks, identification of navigational hazards, for surveying the progress made in dredging operations and other oil and gas explorations activities that require complete coverage of the seabed with critical under keel clearance (Ekpa and Eyoh, 2019; Basil, Hart and Ajayi, 2023).

As shown in Figure 1, the multibeam bathymetric system involves a group of sensors, installed on a survey vessel (Godin, 1998; Hughes, 2018). It comprises a depth-measuring sonar (Figure 1D) incorporated with a positioning system, namely Global Navigational Satellite System (GNSS)

(Figure 1C); a motion sensor, namely, an Inertia Measuring Unit (IMU); and an azimuth sensor (gyroscope) (Figure 1e) (Kaplan and Hegarty, 2017). Figure 1 (A and B) shows the computer and display units. Since the various sensors acquire data in terms of their own unique reference and time frames, the challenge is to integrate the various sensor reference and time frames and transform the vessel frame coordinate system into a terrestrial reference frame (Willian et al., 2022). The integration of the various sensor references and time frames is necessary to minimize systematic errors in the bathymetric data that would result from latency, and calibration uncertainty (Seube and Keyetieu, 2017).

Although the primary purpose of the bathymetric survey is to produce a bathymetric chart to aid in marine transportation systems and to ensure the safety of lives and properties at sea (IHO manual, 2005), in recent times, bathymetric data have been acquired to support exploration and exploitation of ocean resources, to delineate maritime boundaries, to install offshore wind farms; to map the aquatic habitat; to promote marine tourism and as a supportive mechanism in the appropriate exploitation of the blue economy (Mattijs, 2015; IHO manual 2017; Pouce, 2019; Bronner, Sonnewald and Visbeck, 2023). Irrespective of the application of the bathymetric data, the degree of reliability and the associated uncertainty pervading the use of the bathymetric data are of interest to the hydrographic surveyor as no bathymetric measurement is without errors. Errors from the various sensors are propagated horizontally (horizontal propagated uncertainty) and vertically (vertical propagated uncertainty) in the bathymetric data.

The combination of the horizontal and vertical propagated uncertainties delivers the Total Propagated Uncertainty (TPU) of a multibeam system. The latter refers to the cumulative uncertainty in the acquired bathymetric data from the various sensor systems (Battilana and Lawes, 2010). This uncertainty source includes the sound speed variation uncertainty, that results from the refraction of acoustic beams through the water columns (Cordero and Maria, 2018); the time delay (latency) between the various sensors (positional sensor and the IMU sensor), and the computational time delay in the processing software (Bjorn and Einar, 2006); the non-synchronization of sensor frames, amongst others, the multibeam sonar frame and the IMU (Brenna, 2017). More so, the positioning system is also characterized by several errors sources, including, satellite clock and orbital errors, receiver clock errors, tropospheric and ionospheric delays, antenna phase center offset and variation and integer ambiguities and phase delays in carrier phase measurement (Erol et al., 2020; Dodo, Ekeanyanwu and Ono, 2019; Abdallah, 2016) which propagate vertically and horizontally in the measured bathymetric data (Seube, Levilly and Keyetieu-Nlowe, 2015).

In addition, bathymetric measurements are referenced to a vertical datum, which may involve the application of tidal measurements. Tidal gauge uncertainty, including wind effects, and variations in the local gravity field with regard to the distance of the sounding location from the tide gauge instrument, further introduce systematic biases in the bathymetric data (U.S Army

Corps of Engineers, 2013). Furthermore, the acquired bathymetric data contains random errors (e.g., signal noise) which are influenced by environmental and other factors inherent in the design of the acoustic transceivers (Yang, Liu and Zhao, 2004; Dong et al., 2019; Julian et al., 2020).

In order to improve the quality and accuracy of the acquired bathymetric data, the systematic and random errors in the bathymetric system must be accurately modelled, compensated for, and filtered from the bathymetric data (Yang, Liu and Zhao, 2004; Kazimierski and Jaremba, 2023). Systematic errors arising from latency and the non-synchronization of the sensors frames can be eliminated by conducting either a classical or automated patch test, both of which, involve the determination of the boresight angle, expressed in terms of roll, pitch, yaw, and system time delay (latency) (Basil, Hart and Kurotamuno, 2022), while random errors can be filtered by using any of the manual, semi-automated or fully automated filtering techniques (Kalmbach, 2017).

Figure 1(A)

Figure 1(B)

Figure 1(C)

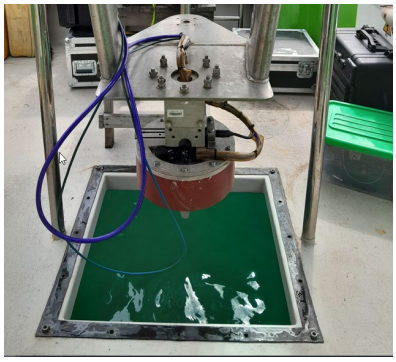

Figure 1(D)


Figure 1(E)

Figure 1: Showing the group of sensors that make up the MBES bathymetric system installed on a survey vessel.

However, the focus of the paper, is to model the systematic biases associated with the integration of the different sensor reference and time frame in the multibeam bathymetric system. This would enhance the quality of the acquired data, and to ensure that error budgeting and uncertainty prediction are effectively carried out during the preparation, acquisition, and

processing stage of the bathymetric exercise to meet the required project specifications and hydrographic standards (IHO, 2020).

## 2. Systems Frames

As shown in Figure 2, the various hydrographic sensor acquires data in their respective reference frame. The positioning sensors (GNSS) acquires data on the Earth-Centre-Earth-fixed (ECEF) geocentric coordinate system (Xu, 2007; Fubara, Fajimirokun and Ezeigbo, 2014); the multibeam sensor acquires data with respect to its reference frame called the multibeam frame; the motion sensor measures the vessel dynamics with respect to the vessel coordinate system, and the gyroscope is configured to measure data with respect to the astronomical coordinate system. Hence, the effective integration of the various sensors requires an adequate knowledge of coordinate transformation from one reference frame to the other (Debese, 2013).

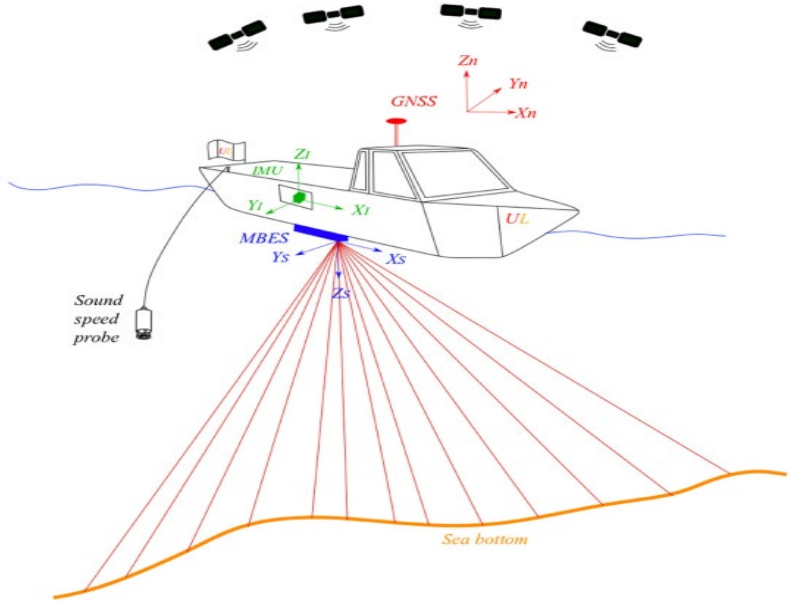


Figure 2: Geometry of the Hydrographic Sensor Frames (Willian et al., 2022).

### 2.1. Multi-beam Frame

The MBES is usually installed in its own frame; multibeam frame, from which, the position and depth information are measured (Figure 2). Owing to the vessel dynamics, the measured bathymetric ranges cannot be accurately converted to equivalent depths by simply applying Equations (1) and (2). For accurate results in these respects, an exact knowledge of the vessel's roll, pitch and heaves which are measured and compensated for by a motion sensor. Furthermore, because the multibeam frame is not in alignment with the IMU frame and the antenna phase centre is also not in perfect alignment with the multibeam phase center, positional errors are likely to arise.

Figure 3: The multibeam Transducer mounted on its Frame

## 2.2. Vessel Reference Frame

Depth determination in a MBES is performed in a vessel in motion and the vessel dynamics must be correctly measured and applied to facilitate accurate representation of the seafloor. The vessel dynamics (roll, pitch, heave) are measured using an IMU mounted on an IMU frame. The IMU is used to define the vessel coordinate system, with the phase centre of the IMU featured as the origin of the coordinate system. As shown in Figure 4, the X-axis points toward the bow of the survey vessel; the Y-axis is right-handed and orthogonal to the X-axis, while the Z-axis is aligned upward in the vertical position.

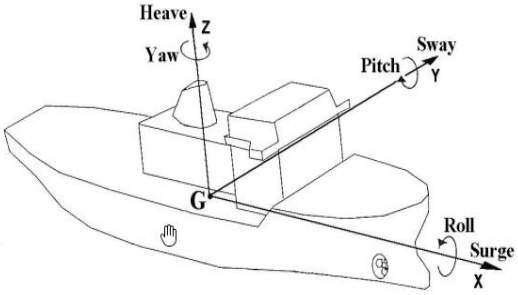


Figure 4: Vessel Reference System ($\boldsymbol{b_I}$) (Santos and Soares, 2007).

The positions of the various sensors (sensor offsets) are measured using the vessel reference system. Interestingly, owing to the moment of force, which is directly proportional to the lever arm offset, the measured roll, pitch, and heaves of the IMU are not equivalent to those experienced by the multibeam sonar.

## 2.3. Terrestrial Reference Frame

The positioning sensor (GNSS receiver) is based on a Terrestrial Reference Frame (TRF). The terrestrial reference frame is an Earth-centre, Earth-fixed (ECEF), right-handed, orthogonal

coordinate system used in describing the position of a point on the Earth's surface (Sebeer, 2003; Jekeli, 2006). Its origin is coinciding with the Earth's centre of mass, its Z-axis coincides with the mean rotational axis of the Earth; its X-axis points to the zero-degree meridian (Greenwich); and its Y-axis is at right angles to both the X-axis and the Z-axis (Torge et al, 2012). The XY plane coincides with the equatorial plane and the XZ plane coincides with the mean zero meridian plane as described in Figure 5.

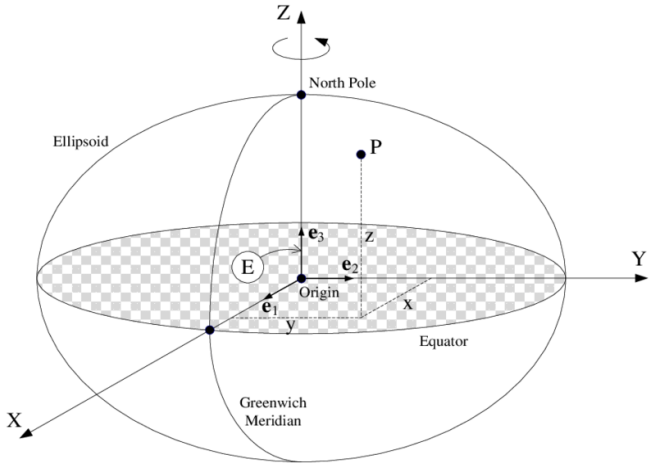


Figure 5: Earth-Fixed-Earth-Centred Reference System (Jekeli, 2006).

### 2.4. Local Geodetic System

Most bathymetric charts are compiled on a flat sheet of paper or in digital format and are mainly represented according to the local (national) coordinate system. The Local Geodetic System (LGS), also called the Local Reference System (LRS), is a projected coordinate system based on an adopted ellipsoidal model that best approximates the national geoid. For Nigeria, the LRS is based on the Clark 1880 ellipsoid, with the topocentric origin (L40) located in Minna, Niger State, Nigeria. The transformation from the ECEF coordinate system to this local datum is based on a unique set of datum transformation parameters (Hart, 2015). This local geodetic coordinate is projected using the Universal Traverse Mercator (UTM) projection system.

## 3. Sounding Position in the MBES Frame

As described in Figure 6, multibeam bathymetric sonar measure ranges are converted to their equivalent depths by applying Equation (1). The bathymetric depth is derived from the two-way travel of an acoustic wave, at a recorded time, using the beam angle as given in Equation (2).

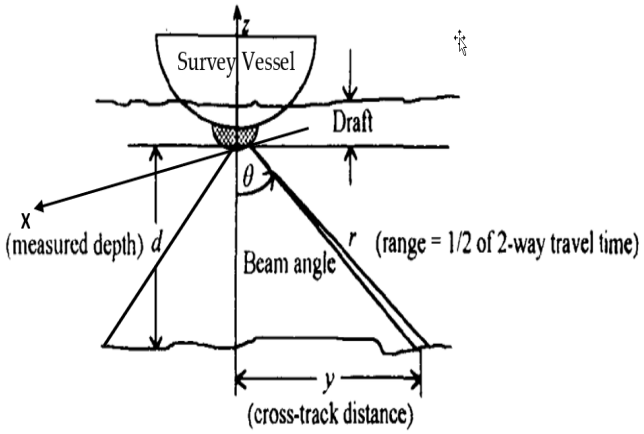


Figure 6: Position and Depth calculated in the Multibeam System (Hare, 2003). (modified).

From Figure 6, the across track distance, ***y***, and the range, ***r,*** from the transducer to the seabed can be computed by applying Equation (2)

$$y = rsin\theta;\ d = rcos\theta = -z \quad (1)$$

$$r = c.dT/2, \quad (2)$$

Where $r$ is the geometric range from the multibeam transducer to the seafloor, d is the equivalent depth (vertical distance) computed using the beam angle $\theta$; dT is the time difference in acoustic transmission from the traducer to the sea bottom and, back to the transceiver The measured depths, (***d***), are based on the multibeam frames which have to be transformed to the vessel coordinate system, to account for the systematic errors resulting from the vessel's roll, pitch, heave and yaw.

### 3.1. Transformation from the Multibeam Frame to the IMU Frame

The transformation from the multibeam frame $(x, y, z)_{bS}$ to the IMU frame $(x, y, z)_{bI}$ is critical in accounting for the vessel dynamics since it is not possible to completely align both frames in perfect synchronization (Brennan, 2017; Basil, Hart and Kurotamuno, 2022). This underscores the need for a patch test to determine the transformation parameters described in terms of roll, pitch, and heading.

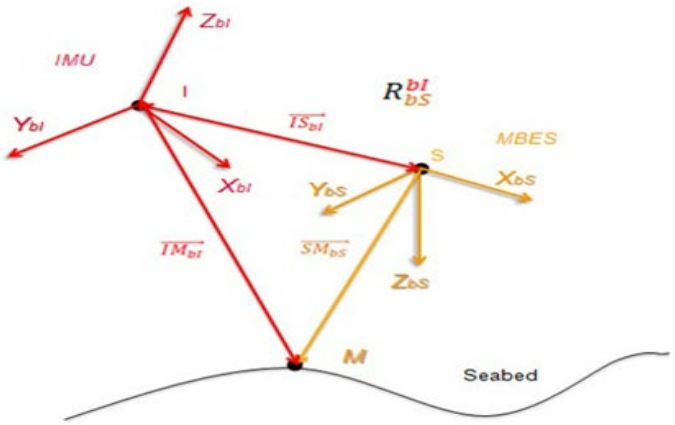


Figure 7: The Sounding Position in the IMU Frame (Wati, Geldof and Seube, 2016).

In Figure 7, the red represents the IMU frame and the yellow represents the Multibeam Frame. Where, $b_i$ is the IMU frame, the origin of the multibeam frame is represented as S, while I defines the origin of the IMU frame, $\overrightarrow{IM_{bi}}$ is the lever arm offset of the IMU frame, and $\overrightarrow{IS_{bi}}$ is the lever arm offset from the origin of the IMU frame to the origin of the MBES frame.

As expressed in Equation (3) the Multibeam Frame is transformed to the IMU frame (Wati, Geldof and Seube, 2016).

$$\overrightarrow{IM_{bi}} = \overrightarrow{IS_{bi}} + R_{bs}^{bi}\overrightarrow{SM_{bs}} \quad (3)$$

$$\text{With, } \overrightarrow{\mathrm{SM_{bi}}} = \mathrm{R_{bs}^{bi}}\overrightarrow{\mathrm{SM_{bs}}} = \mathrm{R_{bs}^{bi}rbs} \quad (4)$$

$$M_{bi} = LA_{IMU}^{MBES} + \mathrm{R_{bs}^{bi}rbs} \quad (5)$$

$R_{bs}^{bi}$ is called the boresight matrix (Le Scouarec et al., 2014). It describes the misalignment angle in roll, pitch, and yaw between the MBES frame and the vessel reference frame. The computation of the boresight matrix $R_{bs}^{bi}$x from the roll bias, $\delta\theta_R$, pitch bias $\delta\theta_P$, and yaw bias, $\delta\alpha$, is presented in Equation 6 (Le Scouarec et al., 2014), which is a function of the three successive rotations described in Figure 8.

$$R_{bs}^{b1} = R\delta\theta_P + R\delta\theta_R + R\delta\alpha \quad (6)$$

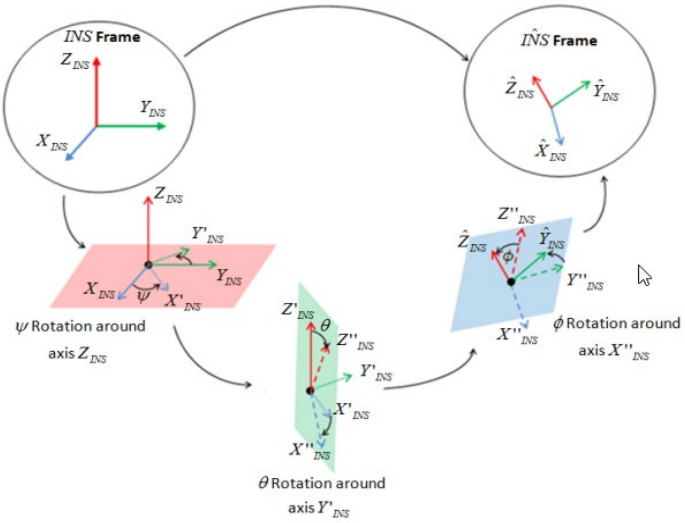


Figure 8: The Boresight Angle description (Le Scouarnec et al., 2014).

Where, $\delta\theta_P, \delta\theta_R,$ and $\delta\alpha$ are systematic biases in pitch, row, and yaw, respectively.

### 3.2. Transformation of Sounding Position from IMU Frame to TRF

In Figure 9, O represents the origin of the terrestrial reference frame, and P represents the phase centre of the GNSS positioning system. $\overrightarrow{OP_{TRF}} = P_{TRF}$ is the phase centre position of GNSS receiver in the TRF, while $LA_{IMU_{bi}}^{GNSS} = \overrightarrow{IP_{bI}}$ represent the lever arm offsets from the IMU frame origin to the phase centre position of GNSS in the IMU frame.

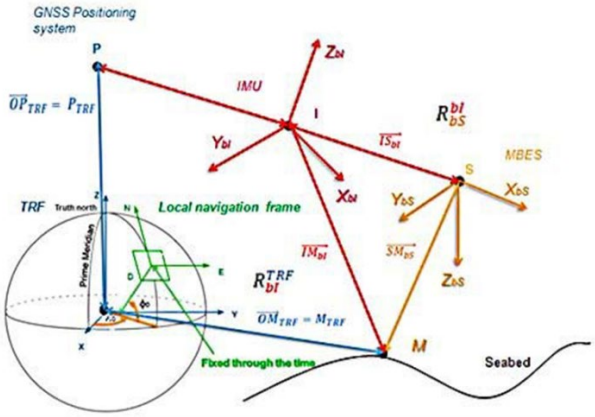


Figure 9: Expressing the Sounding Position in the Terrestrial Frame

The sounding position in the TRF $M_{TRF}$ is expressed as follows (Wati, Geldof and Seube, 2016):

$$\overrightarrow{OM_{TRF}} = M_{TRF} = \overrightarrow{OP_{TRF}} + \overrightarrow{PM_{TRF}} \quad (7)$$

$$\overrightarrow{OM_{TRF}} = \overrightarrow{OP_{TRF}} + R_{bI}^{TRF}\overrightarrow{PM_{bI}} \quad (7b)$$

$$\overrightarrow{PM_{bI}} = LA_{IMU_{bi}}^{GNSS} + LA_{IMU_{bi}}^{MBES} + \mathrm{R}_{\mathrm{bs}}^{\mathrm{b1}}\mathrm{rbs} \quad (8)$$

Therefore,

$$M_{TRF} = \overrightarrow{P_{TRF}} + R_{bI}^{TRF}\left(LA_{IMU_{bi}}^{GNSS} + \mathrm{R}_{\mathrm{bs}}^{\mathrm{b1}}\mathrm{rbs}\right) \quad (9)$$

$R_{bI}^{TRF}$ is the matrix of transformation from the IMU frame to the TRF

$$R_{bI}^{TRF} = \overrightarrow{R_{LGF}^{TRF}}(\lambda, \phi)R_{bI}^{LGF}(\varphi, \theta, \psi) \quad (10)$$

Where:

$\overrightarrow{R_{LGF}^{TRF}}$ is the transformation matrix from the LGF to the TRF.

$R_{bI}^{LGF}$ is the transformation matrix from the IMU to the LGF.

## 4. Effect of the Misaligned Angle on Determined Position and Depth

The misalignment between the MBES frame and the IMU frame is expressed in terms of $\delta\theta_P, \delta\theta_R$, and $\delta\alpha$ which are systematic biases in pitch, roll, and yaw, respectively. Its propagated effects in measured position and depth are discussed in the following sections.

### 4.1. Effect of the Roll Misalignment on Determined Position and Depth

Figure 10 is a schematic diagram of the effect of roll bias, δθ, in a measured range, R. The swathe angle is assumed to be ψ. In reality, it is ψ+δθr, where δθr is the error in the swathe angle resulting from the vessel roll.

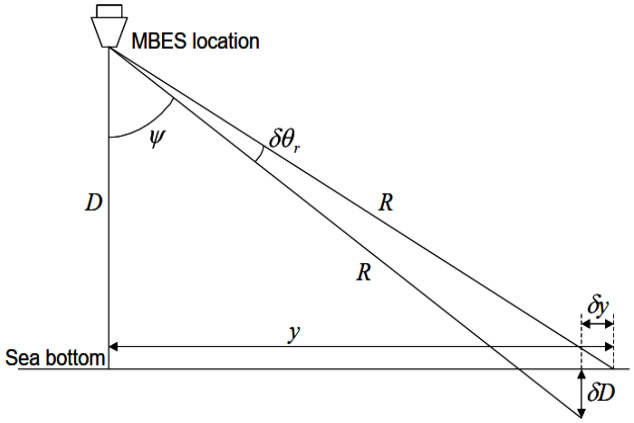


Figure 10: Geometry for a Roll Error Bias

From Figure 10, the slant distance, R, can be mathematically expressed as follows (de Jong et al., 2010):

$$R = \frac{D+\delta D}{cos\psi} = \frac{D}{cos(\psi+\delta\theta_r)} \quad (11)$$

$$R = \frac{y-\delta y}{sin\psi} = \frac{y}{sin(\psi+\delta\theta_r)} \quad (12).$$

where $\delta D$ and $\delta y$ are errors in the measured depth and position, respectively, as a result of the roll bias, $\delta\theta_r$.

For a small roll bias,$\delta\theta_r$ and neglecting the second-order terms, Equations (11) and (12) can be expressed as givens in Equations (13) and (14)

$$\delta D \approx D\delta\theta_r tan\psi \quad (13)$$

$$\delta y \approx -D\delta\theta_r \quad (14).$$

### 4.2. Effect of the Pitch Misalignment on Determined Position and Depth

The systematic error resulting from the pitch biases is described in Figure 11 below.

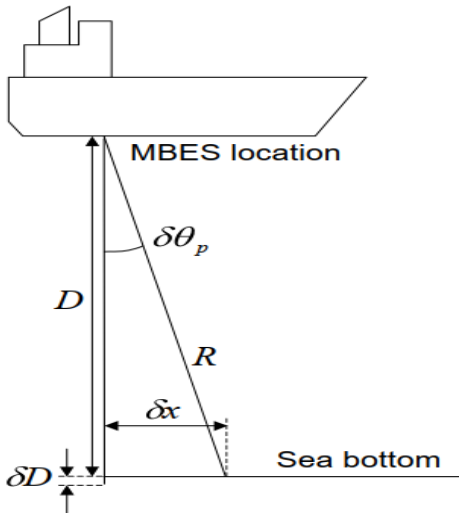


Figure 11: Schematic Diagram for a Pitch Bias, $\boldsymbol{\delta\theta_p}$

From Figure 11, it follows that.

$$R = \frac{D+\delta D}{cos\theta} = \frac{D}{cos(\delta\theta_p)} \quad (15)$$

$$\frac{\delta x}{D} = tan\delta\theta_p \quad (16)$$

Where $\delta x$ is the error in the direction perpendicular to the transmitted beam. It is assumed that the effect of the refraction of sound wave in water has been corrected by measuring the sound velocity profile. Because of the effect of the refraction of sound waves in water, the incident angle $\theta i$ of the sound wave reaching the seafloor is not the beam of the departure angle $\theta s$. Equation (17) and (18) hold true for small pitch bias (de Jong et al., 2010).

$$\delta D \approx \frac{1}{2} D\delta\theta_P^2 \quad (17)$$

$$\delta x \approx D\delta\theta_p \quad (18)$$

Shown in Figure 11 are the errors, $\delta D$, and $\delta x$, as functions of the residual pitch bias, $\delta\theta_p$.

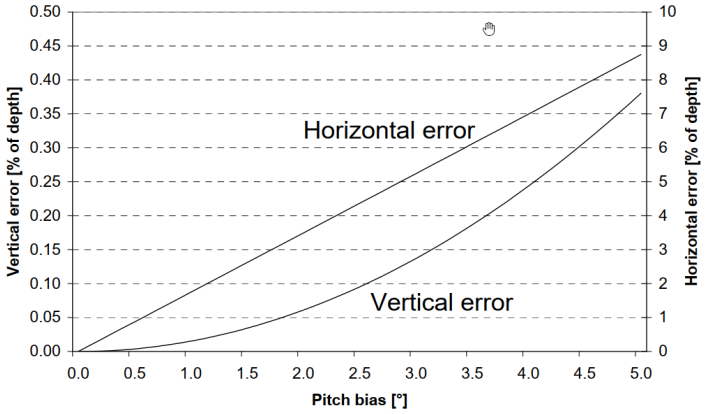


Figure 12: Horizontal and Vertical Positioning Errors as Function of Pitch Bias, $\delta\theta_p$

It can be observed from Figure 12 that the pitch bias is directly proportional to the horizontal error. As noted by (Brennan, 2017), a pitch bias of one degree will propagate to an along-track error in the position of 0.4m when the sonar head is more than 25m above the seabed. The error in the measured depth (vertical error) increases with the swathe angle, that is, the pitch error increases in the outer beams.

### 4.3. Effect of the Yaw Misalignment on Determined Position and Depth

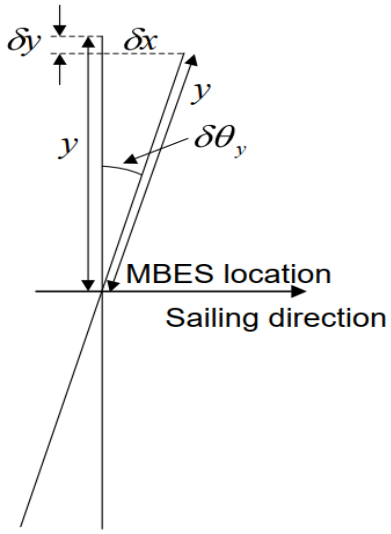


Figure 13: Geometry for a Residual Yaw Bias, $\boldsymbol{\delta\alpha}$

As described in Figure 13 and expressed in Equation (19) and (20), the systematic error in yaw $\delta\alpha$ also results in an error in position.

$$\delta x \approx y\delta\alpha \tag{19}$$

$$\delta y \approx \frac{1}{2}y\delta\theta_P^2 \tag{20}$$

The yaw error describes the azimuth misalignment between the X-axis of the multibeam frame and the gyrocompass. The yaw error is directly proportional to the depth, and the beam angle (Godin, 1998).

### 4.4. Total Propagated Uncertainty (TPU)

The total propagated uncertainty in the multibeam system is the resultant effect, expressed in depth and position, resulting from the systematic basis of the individual sensors and objects. It includes the following:

1. Angular motion sensor contribution, $\sigma_{dAngMot}$, owing to the uncertainties in the roll and pitch measurements and the imperfections in correcting them.
2. Motion sensor and echo sounder alignment contribution, $\sigma_{\mathrm{dAlign}}$, owing to the discrepancies between the roll and the pitch angle measurements of the motion sensor and the transducer.
3. Sound speed contribution, $\sigma_{dss}$, owing to the sound speed uncertainties of the receiving array (for beam forming echo-sounder) and those of the water column (for ray tracing).
4. Heave contribution, $\sigma_H$, owing to the uncertainties in the heave measurements and those from the roll and pitch uncertainties. In the cause of using GNSS for vertical positioning, the uncertainty of heave measurements is replaced by the uncertainty of the vertical component of the GNSS.

From the law of propagation of error, and assuming that the above contributions are uncorrelated random variables, i.e., ignoring the covariance terms, the total propagated uncertainty in the multibeam system is expressed as (Hare, 2003):

$$TPU = \sqrt{\left(\sigma_{\mathrm{dAlign}} + \sigma_{dAngMot} + \sigma_{dss} + \sigma_H\right)} \qquad (21)$$

## 5. Conclusion

Seafloor mapping using a multi-beam echo-sounding system, is gradually becoming the default hydrographic sounding system. This is due to its swathe capability to offer complete coverage of the seabed. However, MBES systems are characterized by several error sources which must be carefully considered for accurate mapping and representation of ocean floor. Analysis of the error budget is critical during the pre-analysis stage of hydrographic survey operations to ensure that the final bathymetric data meet the project specifications and standards. This research provides an exhaustive analysis of the various systematic error sources in a MBES bathymetric system that must be accounted for in the planning, calibration, data acquisition and data processing of multibeam bathymetric data.

## 6. References

Abdallah E. M., (2016). Development of Real-time PPP-Base GPS/INS Integration System using IGS Real-time Service for Hydrographic Surveys. Journal of Surveying Engineering, vol. 142, Issue 2, May 2016.

Basil D. D., Hart L., and Ajayi G. (2023). Marine Geodesy for Hazard Investigation of EDOP production Platform, Akwa Ibom State, Nigeria. In Seyed H. Editor, Applications of Remote Sensing. Intech Open. DOI: 10.5772/intechopen.1001145.

Basil D. D., Hart L., and Kurotamuno J. P., (2022). The Effect of Sonar Misalignment of a Multibeam Hydrographic Surveying. World Journal of Geomatics and Geosciences.

Battilana D., and Lawes G., (2010). Fansweep 20 Total Propagated Uncertainty: Does it reflect Reality? TS 2I – Hydrographic Surveying in Practice with High Resolution Data. FIG Congress. Facing the Challenges Building Capacity, Sydney, Australia.

Bjorn J. and Einar B. (2006). Time Referencing in Offshore Survey Systems. Forsvarets Forskningsinstitutt Norwegian Defense Research Establishment. P O Box 25, NO-2027 Kjeller, Norway.

Brennan, C. W. (2017). R2Sonic LLC Multibeam Training- The Patch Test. Available

Bronner U., Sonnewald M., and Visbeck M. (2023). Digital Twins of the Ocean can foster a sustainable blue economy in a protected marine environment. International Hydrographic Review, vol (29)1.

Cordero Ros, Jose Maria, (2018). "Improved Sound Speed Control through remotely detecting Strong Changes in the Thermocline" master's Theses and Capstones. 1245. Available from: https://scholars.unh.edu/thesis/1245.

de Jong C. D., Lachapelle G., Skone S., and Elema I. A. (2010). Hydrography. Delft University Press. P.O.BOX 98, 2600 MG Delft, The Netherlands. ISBN: 90-407-2359-1.

Debese N. (2013). Bathymetry-sounders, data processing, digital terrain models -Courses and Corrected Exercises (Level C). ISBN

Dodo J. D., Ekeanyanwu U. O., and Ono M. N. (2019). Evaluation of Five Tropospheric Delay Models on Global Navigational Satellite System Measurement in Southern Nigeria Journal of Geosciences, 7(4).

Dong J., Peng R., Li B., Zhu W., and Liwei W. (2019). An Algorithm for Filtering Noise in Multi-beam data based on Rolling Circle Transformation. Advances in Engineering Research, vol 184.

Douglas A. A. (2019). Underwater Acoustic Signal Processing; Modeling, Detection, and Estimation. Springer Nature, Switzerland. ISBN:978-3-319-92983-5.

Ekpa, A. U., Eyoh, E. A. (2019). Analyses of Pre-dredged and Post-dredged Sounding of Odidi Creek in Warri South, Delta State, Nigeria. International Journal of Geoinformatics and Geological Science (SSRG-IJGGS), vol. 6, Issue 2, ISBN: 2393 – 9206

Erol S., Reha M., Ozulu M., and Veli I. (2020). Performance Analysis of Real-time and Post-mission Kinematic Precise Point Positioning in a Marine Environment. Geodesy and Geodynamics 11(1), 401-410.

Fubara M. J., Fajimirokun F. A., Ezeigbo, (2014). Fundamentals of Geodesy. Concept Publication Limited. 77, Shipeolu Street, Palmgrove, Lagos, Nigeria. ISBN: 978-987-525562-1-5.

Godin A. (1998). Calibration of Shallow Water Multibeam Echo-sounding Systems. Master's Report Engineering, Department of Geodesy and Geomatics Engineering Technical Report No. 190, University of New Brunswick, Fredericton, New Brunswick Canada, 182pp.

Hare, R. (2003). Depth and Position Error Budget in Multibeam Echosounding. International Hydrographic Review.

Hart, L. (2015). Development of Datum Transformation Procedure for Nigeria based on National Transformation Version 2 (NTv2) Model. An Unpublished Ph.D. Thesis, submitted to the Department of Geoinformatics and Surveying, University of Nigeria, Enugu Campus, Nigeria.

Hughes J. C., (2018). Multibeam Echosounder. Micallef A., Savini A., and Krastel S. Ed. (2018). Submarine Geomorphology. Springer. ISSN: 2197-9545.

IHO (2020). Standards for Hydrographic Surveys S-44 Edition 6.0.0. Published by the International Hydrographic Organization 4b quai Antoine 1 Principaute de Monaco.

International Hydrographic Organization (2005). Manual on Hydrography. International Hydrographic Bureau 4, Quai Antoine 1er B.P. 445 - MC 98011 MONACO Cedex Principauté de Monaco.

International Hydrographic Organization (2017). Spatial Data Infrastructures: The Marine Dimension. Publication C-17, 2nd Edition.

Jekeli C. (2006). Geometric Reference Systems in Geodesy. Lecture Notes in Geometric Geodesy. Division of Geodesy and Geospatial Science, School of Earth Science, Ohio State University.

Julian L. D., Nathalie D., Thierry S., and Romain B. (2020). A Review of Data-cleaning Approaches in a Hydrographic Framework with a Focus on Bathymetric Multibeam Echosounder Datasets. Journal of Geosciences.

Kalmbach M. (2017). Be Careful with Automatic Filters. Hypack.

Kaplan E. D., and Hegarty C. J. (2017). Understanding GPS/GNSS: Principles and Applications. 3rd Edition. Artech House Publisher. ISBN-13:978-1-63081-058-0.

Kazimierski W., and Jaremba M., (2023). On Quality Analysis of Filtration Methods for Bathymetric Data in Harbour Areas through QPS Qimera Software. Sensors 2023, 23(11), 5076; https://doi.org/10.3390/s23115076

Le Scouarnec R., Touze T., Lacambre J. B., and Seube N., (2014). A new reliable Boresight Calibration Method for Mobile Laser Scanning Application. International Archives of the Photogrammetry, Remote Sensing and Spatial Information Sciences, vol. XL-3/W1, the European Calibration and Orientation Workshop, Castelldefels, Spain.

Mattijs d L., (2015). Surveying for offshore wind. Hydro International Journal. Available from https://www.hydro-international.com/magazines/hydro-international-september-2015.pdf

Ponce R. (2019). Multi-dimensional Marine Data: The next frontier for hydrographic office. International Hydrographic Review, vol. (25)2

Santos T. A., and Soares C. G. (2007). Time domain simulation of ship global loads due to progressive flooding. Advancements in Marine Structures, Taylor and Francis Group, ISBN: 978-0-415-43725-7.

Sebeer G. (2003). Satellite Geodesy, 2nd Edition. Walter de Gruyter. Berlin, ISBN:3-11-0175495.

Seube N., and Keyetieu R. (2017). Multibeam Echo Sounders - IMU Automatic Boresight Calibration on Natural Surfaces. Marine Geodesy 40(2).

Seube N., Levilly S., Keyetieu-Nlowe R. (2015). Automatic 3D Boresight and Latency Estimation of IMU and Multibeam Echo Sounder System. Proceedings of the USHTDRO 15 Conference. National Harbor, Maryland, United States. Hal-03472920.

Torge W. & Muller J. (2012). Geodesy. 4th Edition, Walter de Gruyter, Berlin.

U.S. Army Corps of Engineers (2013). Hydrographic Surveying: Engineering and Design. Washington, DC 20314-1000.

Wati G. N., Geldof J. B., & Seube P. N. (2016). Error Budget Analysis for a Surface and Underwater Survey System. International Hydrographic Review.

Willian N. C., Sylvie D., Éric G., Debese (2022). An Empirical Study of the Influence of Seafloor Morphology on the Uncertainty of Bathymetric Data. Marine Geodesy 45:5, 496-518.

Xu G. (2007). GPS; Theory, Algorithms, and Application. Springer Berlin Heidelberg, New York. ISBN:978-3-540-72714-9.

Yang F, Liu J., and Zhao J. (2004). Detecting Outliers and Filtering Noises in Multi-beam Data. Geomatics and Information Science of Wuhan University, 29(1): 80-83.